

# The Statistical and Physical Properties of the Low Redshift Lyman Alpha Forest Observed with HST/STIS<sup>1</sup>

Romée L. D'Amico<sup>2,3</sup>

Steward Observatory, University of Arizona, Tucson, AZ 85721  
and

Todd M. Tripp<sup>4</sup>

Department of Astrophysical Sciences, Princeton University, Princeton, NJ 08544

## ABSTRACT

We examine the Ly $\alpha$  absorber population at  $z < 0.3$  detected in spectra of the QSOs PG 0953+415 and H 1821+643 taken with the Space Telescope Imaging Spectrograph aboard the Hubble Space Telescope. We compare their statistical properties to those in carefully-constructed mock quasar spectra drawn from a cosmological hydrodynamic simulation of a  $\Lambda$ CDM universe. We find very good agreement in the column density and b-parameter distributions, down to the smallest observable absorbers with  $N_{\text{HI}} \sim 10^{12.3} \text{ cm}^{-2}$ . The observed absorber population is complete for  $N_{\text{HI}} \gtrsim 10^{13} \text{ cm}^{-2}$ , with a column density distribution slope of  $\alpha = 2.04 \pm 0.23$  and a median b-parameter of 21 km/s above this limit. The intergalactic gas giving rise to these weak absorbers is analogous to that at high redshift, located in diffuse large-scale structures that are highly photoionized by the metagalactic UV flux, though a greater number arise within shock-heated warm gas. The density, temperature, and column density of these absorbers follow similar relationships to those at high redshift, though with substantially larger scatter due to the shock-heated gas. The b-parameters typically have a significant contribution from thermal broadening, which facilitates a measurement of the low- $z$  IGM temperature as traced by Ly $\alpha$  absorbers. From our simulation we estimate  $T_{\text{IGM}} \sim 5000 \text{ K}$ , with an upper limit of  $10^4 \text{ K}$ , at the mean density. The agreement in predicted and observed amplitude of the column density distributions allows us to measure the H I photoionization rate at  $z = 0.17$  to be  $\Gamma_{\text{HI}} = 10^{13.3 \pm 0.7} \text{ s}^{-1}$  (estimated modeling uncertainty), close to predictions based on quasar properties.

Subject headings: cosmology: observations | cosmology: theory | intergalactic medium | quasars: absorption lines | quasars: individual (PG 0953+415, H 1821+643)

## 1. Introduction

Neutral hydrogen along the line of sight to distant quasars produces numerous Lyman  $\alpha$ -

Ly $\alpha$  absorption features in quasar spectra, known as the Ly $\alpha$  "forest" (Lynds 1971). At redshifts  $z \lesssim 2.5$ , high-resolution optical spectroscopy with HIRES (Vogt et al. 1994) on the Keck 10m telescope has enabled the statistics of Ly $\alpha$  absorbers to be determined to high precision (Hu et al. 1995; Lu et al. 1996; Kim et al. 1997; Kirkman & Tytler 1997). Recent observations using UVES at the VLT have probed absorbers at redshifts  $1.5 \lesssim z \lesssim 2.5$  (Kim, Cristiani & D'Ondico 2000). In conjunction with these

<sup>2</sup>rad@as.arizona.edu

<sup>3</sup>Hubble Fellow

<sup>4</sup>tripp@astro.princeton.edu

<sup>1</sup>Based on observations with the NASA/ESA Hubble Space Telescope, obtained at the Space Telescope Science Institute, which is operated by the Association of Universities for Research in Astronomy, Inc., under NASA contract NAS 5-26555.

observations, hydrodynamic simulations of the intergalactic medium (IGM) have forwarded a self-consistent physical picture for the origin of Ly forest absorbers ( $N_{\text{HI}} \sim 10^{17} \text{ cm}^{-2}$ ), in which they arise from highly photoionized gas tracing the dark matter potentials in mildly nonlinear large-scale structures (for a review, see Rauch 1998). Though the absorbing gas is typically out of dynamical and thermal equilibrium, a relatively simple relation known as the Fluctuating Gunn-Peterson Approximation (FGPA; for the full expression see Croft et al. 1998) captures the essential physics of optically-thin Ly absorbers:

$$\tau_{\text{Ly}\alpha} \approx 1.6 \tau_{\text{HI}}^{-1}; \quad (1)$$

where  $\tau_{\text{Ly}\alpha}$  is the Ly  $\alpha$  optical depth,  $\rho_b$  is the local density of baryons (assumed to trace the dark matter), and  $\Gamma_{\text{HI}}$  is the HI photoionization rate. The FGPA has been utilized in various forms to constrain many physical parameters associated with high-redshift Ly forest absorption, such as a measurement of  $b$  (Rauch et al. 1997; Weinberg et al. 1997) and the mass power spectrum at  $z \sim 3$  (Croft et al. 1998; McDonald et al. 2000a), and implicitly in the determination of the metallicity of the diffuse IGM (Rauch, Haehnelt, & Steinmetz 1997; Davé et al. 1998) and the "equation of state" of the IGM (Hui & Gnedin 1997; Schaye et al. 1999; McDonald et al. 2000a).

At redshifts  $z \sim 1.5$ , the Ly transition falls in the ultraviolet, requiring more challenging space-based observation. The Hubble Space Telescope (HST) Quasar Absorption Line Key Project (Bahcall et al. 1993, 1996) obtained UV quasar spectra for a large sample of quasars (Jannuzi et al. 1998) using the HST Faint Object Spectrograph (FOS). Unlike Keck/HIRES, FOS is unable to resolve individual Ly absorption features, having a resolution of  $\sim 230 \text{ km/s}$ . Nevertheless, this sample greatly expanded our understanding of the properties and evolution of Ly forest absorbers from  $z \sim 1.7$  to  $z \sim 0$ . One surprising result was that the rate of evolution of absorbers slows dramatically at  $z \sim 2$ ; this was initially indicated by the large number of Ly lines detected in the first observations of 3C 373 (Morris et al. 1991; Bahcall et al. 1991) and combined with a larger number of sight lines from the FOS Key Project (Bahcall et al. 1996). Cosmological hydrodynamic simulations suggested that this was a result of the dim-

ishing ionizing background in concert with the decline in the quasar population after  $z \sim 2$  (Theuns, Leonard, & Efsthathiou 1998; Davé et al. 1999, hereafter DHKW). FOS data also suggested that high-column density absorbers are evolving away faster than low-column density ones (Weymann et al. 1998), which DHKW suggested was due to the increase in the relative cross-section of lower-column absorbing gas. DHKW also showed that the observed correlation between absorber equivalent width and impact parameter (Chen et al. 1998; Tripp, Lu, & Savage 1998) arises purely due to the clustering of matter, not due to a physical association of absorbers with HI in large gaseous halos of individual galaxies. Thus qualitatively, Ly absorbers at low redshift are well-described by current structure formation models. Still, due to the low resolution of FOS and the computational difficulty of running simulations to  $z = 0$ , a detailed quantitative agreement of simulations with observations analogous to that obtained at high redshift has yet to be achieved.

HST's Goddard High Resolution Spectrograph (GHRS) has yielded some complementary results regarding low- $z$  Ly absorbers. In the intermediate-resolution mode usually employed in QSO absorption line studies, the GHRS provided an instrumental resolution of  $\sim 19 \text{ km/s}$ , which is comparable to the widths of Ly lines, making a determination of individual absorber column densities and  $b$ -parameters possible, though not straightforward (Penton, Shull, & Stocke 2000). The Far Ultraviolet Spectroscopic Explorer (FUSE) can be used to detect higher Lyman series lines at wavelengths shortward of the HST bandpass and thereby enable a curve-of-growth analysis to more accurately estimate line widths (Shull et al. 2000). The resulting widths were typically half of that obtained by direct profile fitting of GHRS data, which Shull et al. (2000) interpreted as an indication of non-thermal components in Ly absorbers.

The deployment of the Space Telescope Imaging Spectrograph (STIS) aboard HST has significantly improved our ability to study low-redshift Ly absorbers. The intermediate-resolution FUV echelle mode of STIS has a resolution of  $7 \text{ km/s}$  FWHM and enables detection of absorbers with  $N_{\text{HI}} \sim 10^{13} \text{ cm}^{-2}$ . This resolution, similar to that of Keck/HIRES, allows virtually all Ly absorbers

to be fully resolved, facilitating a robust comparison with high-resolution hydrodynamic simulations. In this paper we determine the column density and linewidth distributions from STIS spectra of quasars PG 0953+ 415 ( $z_{\text{em}} = 0.239$ ) and H 1821+ 643 ( $z_{\text{em}} = 0.297$ ), and we compare them to carefully-constructed mock quasar spectra drawn from a cosmological hydrodynamic simulation of a  $\Lambda$ CDM universe. We find that the agreement between simulations and observations is quite good, and lends strong support to the physical picture of the low-redshift intergalactic medium provided by hierarchical structure formation models.

DHKW suggested that the physical state of the gas giving rise to Ly absorption at low redshift is fundamentally similar to that at high redshift, with the exceptions that a dynamically equivalent patch of gas at low redshift gives rise to an absorber with significantly lower column density (see their Figure 10), and collisionally ionized hot gas plays an increasingly important role to lower redshift. With STIS data, we can now probe these low- $N_{\text{HI}}$  absorbers that are predicted to be physically similar to the high- $z$  forest absorbers. If the FGPA provides a reasonable description of weak low- $z$  absorbers, it may be possible to apply many of the same techniques used to determine physical properties of the IGM at high redshift to STIS data. In this paper we present such applications, including an estimate of the extragalactic H I photoionization rate. Despite large systematic uncertainties in the modeling, our measurement is among the most sensitive to date.

In §2 we describe the STIS observations of the two low-redshift quasars, the hydrodynamic simulations we will use for comparison, and the construction and analysis of artificial spectra. In §3 we present the column density and linewidth distribution from STIS data alongside the distributions from carefully-constructed artificial spectra. In §4 we explore the physical state of gas giving rise to the sorts of absorbers seen in these STIS spectra, and make a preliminary determination of the IGM temperature from the observed  $N_{\text{HI}}$  distribution. In §5 we constrain the average metagalactic photoionizing flux incident on these absorbers by matching the amplitude of the column density distribution to observations. We present our conclusions in §6.

## 2. Simulation and Observations

### 2.1. STIS Quasar Spectra

The STIS observations of PG 0953+ 415 and H 1821+ 643 were obtained by Tripp & Savage (2000) and Tripp, Savage, & Jenkins (2000) to study low-redshift O VI absorbers as well as the relationships between the various types of absorption systems and galaxies. After the publication of those papers, more observations were obtained, and modest improvements in the data reduction procedures were implemented. A detailed description of the observations, data reduction, and complete line lists are found in a separate paper (Tripp et al. 2001). Here we provide a brief summary.

Both QSOs were observed with the medium-resolution FUV echelle mode ( $\approx 140\text{M}$ ). H 1821+ 643 was observed with the  $0^{\circ}2 \times 0^{\circ}06$  slit, while PG 0953+ 415 was observed with the  $0^{\circ}2 \times 0^{\circ}2$  slit for better throughput. This STIS mode provides a resolution of  $R = \lambda/\Delta\lambda = 46,000$  ( $7 \text{ km/s}$  FWHM) with the  $0^{\circ}2 \times 0^{\circ}06$  slit (Kinble et al. 1998); the FWHM is only slightly degraded with the  $0^{\circ}2 \times 0^{\circ}2$  slit, but the broad wings of the line spread function are more prominent (see Figure 13.87 in the STIS Instrument Handbook, v4.1). This mode provides spectra extending from 1150

1710 Å with only a few small gaps between orders at  $\lambda > 1630 \text{ Å}$ , redwards of the Ly forest.

The data were reduced with the STIS Instrument Definition Team software. The individual spectra were flatfielded, extracted, and wavelength and flux calibrated with the standard techniques. Then a correction for scattered light was applied using the method developed by the STIS Team, and the individual spectra were combined with weighting based on signal-to-noise ratio (S/N). Finally, overlapping regions of adjacent orders were also coadded weighted by S/N.

### 2.2. Generation of Artificial Spectra

We employ a cosmological hydrodynamic simulation of a  $\Lambda$ -dominated cold dark matter model, run with PTreesPH (Dave, Dubinski & Hernquist 1997), having  $\Omega_b = 0.0473$ ,  $\Omega_{\text{CDM}} = 0.3527$ ,  $h = 0.65$ ,  $H_0 = 65 \text{ km s}^{-1} \text{ Mpc}^{-1}$ , inflationary spectral index  $n = 0.95$ , and rms fluctuation amplitude  $\sigma_8 = 0.8$ . We use  $64^3$  dark matter particles and  $64^3$  gas particles in a periodic cube  $11.111 h^{-1} \text{ co}$

moving  $Mpc$  on a side and a gravitational softening length of  $3.5h^{-1}$  comoving kpc (equivalent Plummer softening). Further details may be found in DHKW. We choose  $\rho_b$  to match recent observations of the deuterium abundance (Burles & Tytler 1998), and adopt a UV background from Haardt & Madau (1996). In post-processing we adjusted the intensity of the UV background slightly in order to match the evolution of the number density of absorbers ( $dN/dz$ ) with rest equivalent width  $W_r > 0.24A$  (the matched LCDM curve in Figure 4 of DHKW), by assuming the optical depth in artificial spectra is inversely proportional to the photoionization rate. This simulation is otherwise the same as the LCDM run in DHKW.

From this simulation we generate artificial spectra whose characteristics closely model those of PG 0953+415 and H 1821+643; see Dave et al. (1998) for a more detailed description of this procedure. We assume zero metallicity, so all features in the artificial spectra are Lyman series lines. The flux is interpolated to the wavelength of each pixel in the observed spectrum, and Gaussian random noise is added based on the noise value at the nearest pixel in the observed spectrum with a similar flux. We convolve the spectrum with the STIS line spread function of the slit used to observe each quasar, interpolated to the pixels' wavelength. We fit a continuum to both observed and artificial spectra using a median filter in a sliding 100-pixel ( $\sim 300$  km/s) window. We adjust the median filter so that in each set of artificial spectra, there is on average no net flux subtracted by the continuum fitting (i.e. we recover the true continuum, on average). We generate 20 artificial spectra for each quasar, for a total of 40.

We fit Voigt profiles to the observed and artificial spectra using AutoVP (Dave et al. 1997). We choose a 4.5 detection threshold for identifying Ly absorbers, using the procedure described in Lanzetta, Tumshak, & Wolfe (1987) with a 20 km/s detection window. We only consider lines between the Ly and Ly emission peaks so as to reduce confusion with higher-order Lyman series and metal lines, and do not include any absorbers within 5000 km/s of the Ly emission peak. Spectral regions containing Galactic ISM lines or extragalactic metal lines identified in the data are discarded, and any lines identified in the artificial spectra in those wavelength regions are dis-

carded as well, ensuring that each artificial spectrum has the same redshift path length as its corresponding quasar spectrum. Note that considerable care must be exercised in the identification of the Milky Way features since the spectra have sufficient sensitivity to show weak ISM lines such as the C I and Ni II resonance transitions; similarly, several extragalactic metal lines are present in the wavelength range of interest (see Tripp, Savage, & Jenkins 2000; Tripp et al. 2001).

An 80Å sample of H 1821+643 is shown in Figure 1, at three stages. The first (top panel) shows the unnormalized observed spectrum, with the continuum fit as the thick solid line, and the 1 noise vector at the bottom. The middle panel shows the normalized spectrum with Voigt profile identifications indicated by the tick marks (some of the marked lines are Milky Way or extragalactic metal lines which are discarded). The bottom panel shows the corresponding segment from an artificial H 1821+643 spectrum, with the same analysis procedure having been applied.

While there may be biases associated with our particular continuum fitting, line identification, and Voigt profiling algorithms, the application of the identical routines to both simulations and observations facilitates a fair comparison between the two. We do not expect these biases to be significant since we are fully resolving virtually all Ly absorbers, and continuum fitting is relatively straightforward since the low- $z$  forest is sparse. Any systematic biases that do arise will, in most cases, be reflected equally in the statistics of both the simulations and observations.

Our  $11:11h^{-1}Mpc$  simulation volume is small compared to the scale of linearity at  $z = 0$ , hence our derived statistics are subject to cosmic variance. We do not attempt to estimate this, since to do so would require running a suite of simulations that is beyond our current capabilities. We note that our randomly chosen volume is typical, containing no anomalously large mass concentrations or voids. As we will show, most Ly absorbers arise in moderate overdensity regions that are well-sampled even within our small volume, though the contribution from coupling to waves larger than our boxsize is not included. We leave a systematic study of these effects for future work.

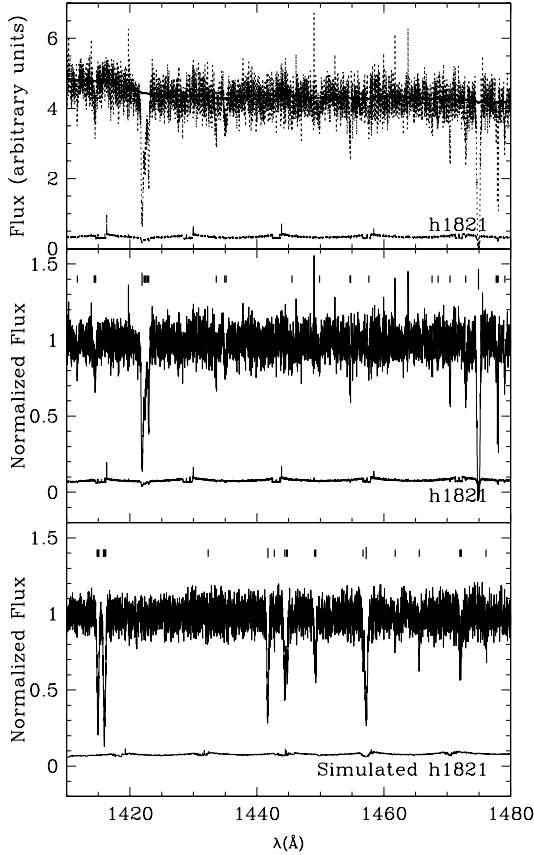


Fig. 1. | An 80Å segment from the Ly forest of H1821+643. Top panel shows the unnormalized spectrum with continuum fit. Middle panel shows the normalized spectrum with line identifications by AutoVP. Note that some of the marked lines in this panel are not Ly lines, e.g., the Si III 1206.5Å lines at  $z = 0.225$  (see Figure 2 in Tripp, Savage, & Jenkins 2000) and the Milky Way Ni II line at 1454.8Å. Bottom panel shows an artificial H1821+643 spectrum mimicking its resolution and noise characteristics, continuum fit and analyzed with the same routines applied to the H1821+643 spectrum. The  $1\sigma$  noise vector is shown near the bottom of each panel.

### 3. Absorber Statistics

The distributions of column densities and Doppler widths  $b$  obtained by fitting Voigt profiles to spectral features have historically been used to characterize the statistics of Ly forest absorbers. Though these statistics reflect the old paradigm that Ly absorbers arise from isolated thermally-broadened clouds, an assumption that is likely to be incorrect in detail (e.g. Hemquist et al. 1996; Outram, Carswell & Theuns 2000; Theuns, Schaye, & Haehnelt 2000), such statistics still represent a fair statistical characterization of the absorber population, more so at low redshift than at high redshift because line blending is less severe and individual absorbers can more easily be identified.

At high redshift, statistics based on the distribution of flux in the Ly forest have gained favor (e.g. McDonald et al. 2000a; Machecek et al. 2000) due to their simplicity, ease of implementation, and robustness of comparison with models. At low redshift, these statistics are somewhat more difficult to apply reliably, because they require that the opacity in the forest be predominantly due to Ly absorption, whereas at low- $z$  the relative contribution from metal and ISM lines is greatly increased. Thus we will leave flux statistics for future work, and focus here on Voigt profile statistics.

We identify 33 Ly absorption lines in the Ly region of PG0953+415, and 56 in H1821+643, using AutoVP. There are more absorbers in H1821+643 because the average signal-to-noise ratio per  $3 \text{ km/s}$  pixel in this wavelength range is higher,  $S/N = 13:7$  compared to 8:1 for PG0953+415, so more weak absorbers are identified. The total redshift path length is  $z = 0.165$  for PG0953+415 and  $z = 0.170$  for H1821+643, not including discarded regions that cover  $z = 0.008$  and  $z = 0.011$ , respectively. This path length is for absorbers above our completeness limit, which we will show is  $N_{\text{HI}} \lesssim 10^{13} \text{ cm}^{-2}$ ; for weaker absorbers, the effective path length is smaller (see, for example, the discussion in Penton, Shull, & Stocke 2000), but by construction is still identical in the data and the artificial spectra. We will only quote statistics for absorbers above our completeness limit. The mean redshift of our entire absorber sample

is  $z = 0.17$ .

### 3.1. Column Density Distribution

The column density distribution is defined as the number of lines per unit redshift  $z$  per unit column density  $N_{\text{HI}}$ , and is generally parameterized as a power law in  $N_{\text{HI}}$ ,

$$f(N_{\text{HI}}) = \frac{d^2N}{dzdN_{\text{HI}}} / N_{\text{HI}} : \quad (2)$$

At  $z \approx 2.5$ ,  $\alpha = 1.5$  (Hu et al. 1995; Lu et al. 1996; Kirkman & Tytler 1997; Kim et al. 1997). Recent work with VLT/UVES suggests a similar slope ( $\alpha = 1.4$ ) down to  $z = 1.5$  (Kim, Cristiani & D’Orazio 2000). This is predicted to steepen significantly at low redshift (Zhang, Aninos & Norman 1995; Theuns, Leonard, & Efsthathiou 1998, DHKW). GHRs observations by Penton, Shull, & Stocke (2000) indicate a somewhat steeper slope of  $\alpha = 1.8$ , but that was obtained by assuming a particular  $b$  for all absorbers (varied between 20 and 30 km/s) rather than by determining  $b$  and  $N_{\text{HI}}$  independently from profile fitting. An alternative statement of this trend is that high- $N_{\text{HI}}$  absorbers are predicted to evolve away faster than low- $N_{\text{HI}}$  ones. The analysis in x5.2 of Penton, Shull, & Stocke (2000) suggests no significant difference between the evolution of absorbers with  $10^{13.1} < N_{\text{HI}} < 10^{14} \text{ cm}^{-2}$  and  $N_{\text{HI}} < 10^{14} \text{ cm}^{-2}$ , contradicting FOS results (Weymann et al. 1998) as well as model predictions. However, Figure 18 of Penton, Shull, & Stocke (2000) suggests that between  $10^{13} < N_{\text{HI}} < 10^{14} \text{ cm}^{-2}$ , stronger absorbers evolve away significantly faster than weaker ones from  $z = 3$  to 0.

Figure 2 shows the column density distribution of identified absorbers in the two STIS spectra (combined) along with the corresponding results from 40 artificial spectra. The simulations and observations show very good agreement, in both the slope and the amplitude of  $f(N_{\text{HI}})$ . The best-fit slopes for  $N_{\text{HI}} > 10^{13} \text{ cm}^{-2}$  are  $\alpha_{\text{obs}} = 2.04 \pm 0.23$  and  $\alpha_{\text{sim}} = 2.15 \pm 0.04$ . Thus we find that the column density distribution has steepened considerably since  $z = 3$ , at least for absorbers with  $10^{13} < N_{\text{HI}} < 10^{14} \text{ cm}^{-2}$ , in general agreement with Figure 18 of Penton, Shull, & Stocke (2000). We do find a slope that is somewhat steeper (by  $\sim 1$ ) than that found from the GHRs sample (Penton, Shull, & Stocke 2000). Note that we

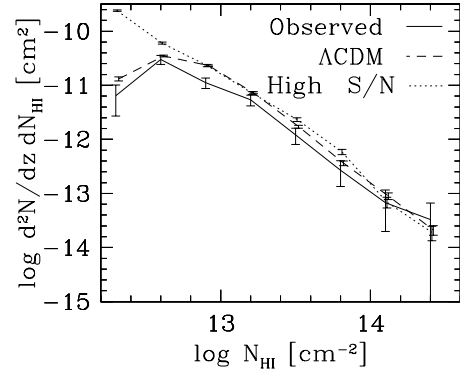


Fig. 2. | Column density distributions from observations of PG 0953+ 415 and H 1821+ 643 (solid line) and a sample of 20 artificial spectra for each quasar (dashed line). Dotted line shows the result from artificial spectra with S/N increased by 5, indicating that the absorber population is complete down to at least  $N_{\text{HI}} = 10^{12.9} \text{ cm}^{-2}$ . Note that the ionizing background used to generate the artificial spectra was normalized to the evolution of absorbers in the Key Project FOS sample (see DHKW), and is not the the normalization that best fits this STIS sample; we will quantify this further in x5.

only include  $N_{\text{HI}} = 10^{12.9} \text{cm}^{-2}$  bins in this plot; had we included the bin at  $N_{\text{HI}} = 10^{12.6} \text{cm}^{-2}$ , the slopes would reduce to  $\sim 1.7$ . This bin is only slightly incomplete (as we discuss below), but it illustrates that completeness must be carefully assessed before an accurate determination of  $\alpha$  can be made.

The dotted line in Figure 2 shows the column density distribution for a set of artificial spectra where the S/N ratio has been increased by a factor of 5, allowing weaker absorbers to be identified. No significant differences are seen for  $N_{\text{HI}} > 10^{12.9} \text{cm}^{-2}$ . This tests the completeness of the observations (and simulations) at low  $N_{\text{HI}}$ , showing that the absorber sample in PG 0953+415 and H 1821+643 is complete down to  $N_{\text{HI}} = 10^{13} \text{cm}^{-2}$ , and  $\sim 70\%$  complete to  $N_{\text{HI}} = 10^{12.6} \text{cm}^{-2}$ . The similar shape of the turnover below this value indicates that the noise level in the artificial spectra are faithfully mimicking that in the STIS data.

The agreement in amplitude of  $f(N_{\text{HI}})$  depends on the chosen value of the H I photoionization rate used to generate the artificial spectra, as we will explore further in §5. The best-fit amplitudes for the simulated and observed absorbers are  $f_{\text{sim}}(10^{13} \text{cm}^{-2}) = 10.70 \pm 0.02$  and  $f_{\text{obs}}(10^{13} \text{cm}^{-2}) = 10.87 \pm 0.12$  respectively. Recall that the ionizing background was set to obtain agreement with  $dN/dz$  of absorbers with  $W_r > 0.24A(N_{\text{HI}} > 10^{14} \text{cm}^{-2})$  measured by the Key Project's sample of FOS quasar spectra (see Davé et al. 1999), which probes a different column density regime than these STIS spectra. The general agreement between these independent data sets lends further support to the overall model.

### 3.2. Distribution of b-parameters

The b-parameter distribution has historically provided a significant challenge for theories of the Ly forest. At high redshift, absorbers are predominantly broadened by bulk flow (e.g. Hemquist et al. 1996; Outram, Carswell & Theuns 2000), but thermal broadening is not negligible (Theuns, Schaye, & Haehnelt 2000). Hence the b-parameter distribution can probe the temperature of Ly forest gas (Schaye et al. 1999; McDonald et al. 2000b; Ricotti, Gnedin & Shull 2000). The derived temperatures seem to suggest that intergalactic gas at  $z \sim 3$  is heated by some other process in addition to equilibrium

H I photoionization, such as helium reionization (Haehnelt & Steinmetz 1998). Though some observational constraints are beginning to emerge (Heap et al. 2000; Songaila & Cowie 1996; Giroux & Shull 1997), theories for when and how reionization occurs are quite uncertain, making an a priori prediction of b-parameters difficult. Furthermore, it has been shown that a robust prediction of the b-parameter distribution for comparison with Keck/HIRES data requires exceptionally high numerical resolution (Theuns et al. 1998; Bryan et al. 1999), higher for instance than in the simulation analyzed here.

At low redshift, it is unclear whether simulation predictions of b-parameters are more or less robust. Certainly reionization is far enough in the past that the IGM is expected to have returned to an equilibrium ionization condition. However, the character of the low- $z$  IGM has changed dramatically. In particular, though a substantial fraction of the baryons remains in cool, photoionized gas, a significant component of intergalactic gas now resides at temperatures exceeding that from photoionization, due to shock heating from infall onto large-scale structure (DHKW; Cen & Ostriker 1999; Davé et al. 2001, hereafter D01). Furthermore, it is possible that non-thermal processes such as supernova heating also heat the IGM (Wu, Fabian, & Nusser 2000, though see D01 and Croft et al. 2000). The simulation used here includes these physical processes (it is simulation \textit{D2} in D01), but they are more complex than just photoionization heating and adiabatic cooling, involving highly uncertain theoretical issues such as escape fraction of feedback energy and the contribution of small-scale shocks to IGM heating (see D01 for discussion). Furthermore, the baryonic mass fraction in various intergalactic components depends on  $\Omega_b$  and cosmology (DHKW) in a way that is difficult to predict analytically, as we will discuss in §5.

With these caveats in mind, we present in Figure 3 a comparison of the b-parameter distribution in our two STIS quasar spectra and the artificial spectra. We only show the distribution for absorbers above our completeness limit of  $N_{\text{HI}} > 10^{13} \text{cm}^{-2}$ , but including absorbers down to  $N_{\text{HI}} = 10^{12.6} \text{cm}^{-2}$  makes little difference in the results. Remarkably, despite all the potential pitfalls, the agreement between simulations

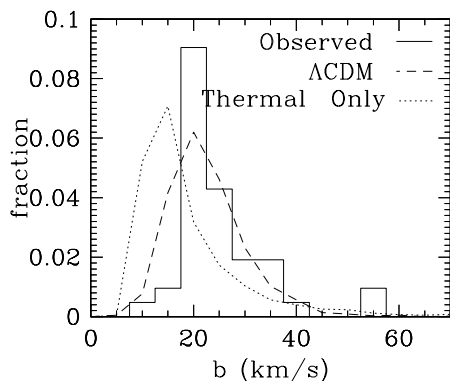


Fig. 3. | b-parameter distribution from observations (solid line) and artificial spectra (dashed line). The dotted line shows the distribution of thermal widths for the absorbers in the artificial spectra, discussed in §4.3. Only lines with  $N_{\text{HI}} > 10^{13} \text{cm}^{-2}$  are included.

and observations is quite good. The median b-parameter is observed to be 22 km/s, while the simulations predict 21.5 km/s. The average b is observed to be 25 km/s, and predicted to be 23 km/s. A K-S test shows no statistically significant difference between the b distributions from the observations and simulations. These quoted values include the contribution from the STIS line spread function; correcting for this lowers these values by 1 km/s, yielding an intrinsic median b-parameter of 21 km/s. The dotted line shows the distribution of thermal widths for the artificial sample, which we will discuss in §4.3.

The median b value is lower than the 27–36 km/s typically found at  $z = 2.5-4$  (Kim et al. 1997), though a higher S/N spectrum finds somewhat lower b values (Kirkman & Tytler 1997). This is qualitatively consistent with the prediction that the unshocked IGM is cooler at low- $z$  due to the lowered intensity of the photoionizing background, but could also be a result of lowered bulk flow broadening due to differential Hubble expansion across the absorbing structures. We will explore the relative importance of these effects in §4.3.

Our b-parameters do not follow an extrapolation of the trend seen by Kim et al. (1997), that b generally increases with decreasing redshift for  $2.1 < z < 4$ . They are also significantly smaller than b-parameters derived from probing GHRs data ( $b = 38-16$  km/s, Penton, Shull, & Stocke 2000). On the other hand, we are in agreement with a curve-of-growth analysis using FUSE and GHRs data by Shull et al. (2000), who find  $b = 31-7$  km/s and  $b_{\text{median}} = 28$  km/s. As we will discuss further in §4.3, larger column density absorbers are wider, and Figure 6 shows that at the median  $N_{\text{HI}} = 10^{14.2} \text{cm}^{-2}$  of the Shull et al. (2000) sample, our median b-parameter is 30. This agrees quite well with their value of 28 km/s, given the small samples involved. Our STIS data probes weaker lines than the FUSE sample, and hence results in a smaller median b.

Shull et al. (2000) find that, for partially saturated lines, direct probing of GHRs data overestimates the b-parameter by a factor of two on average, and thereby calls into question the validity of probing. It is true that results from probing a saturated Ly line can have large uncertainties. However, the vast majority of our

lines are not saturated ( $N_{\text{HI}} \sim 10^{14} \text{cm}^{-2}$ ), so our statistics, particularly our median  $b$  value, should not be too sensitive to this effect. Furthermore, as evidenced by our agreement with the curve-of-growth study of Shull et al. (2000), we are at most only slightly overestimating  $b$ -parameters. The 7 km/s resolution of our data insures that we can adequately sample individual Ly absorbers profiles, since the smallest Ly absorber widths are significantly larger. Note that we do find a number of metal and ISM lines that have widths comparable to the resolution (Tripp, Savage, & Jenkins 2000; Tripp et al. 2001), indicating that if such Ly lines existed, they would have been detected.

The agreement of the predicted and observed  $b$ -parameter distributions is actually better than that obtained in a similar comparison at high redshift (Dave et al. 1997). This surprising result may be because STIS observations do not yet have high enough S/N to show discrepancies with the simulations. Or it may be that since low- $z$  forest requires less deblending of absorption features, the  $b$ -parameter distribution is more robustly predicted. Alternatively, we may have simply been fortunate with this simulation, and future higher-resolution, larger-volume simulations will show discrepancies. For now we are encouraged by the good agreement, and will proceed on the assumption that it is not a spurious coincidence, but rather reflects the basic validity of the underlying physical model.

#### 4. Physical Properties of Ly Absorbers

The good agreement between the observed and simulated absorber statistics suggests that the simulations are accurately describing the origin of weak Ly absorbers at low redshift. In this section, we investigate the physical conditions in the simulated IGM that give rise to weak Ly absorbers. These studies are similar in spirit to those in DHKW, but with a focus on the weak absorber population seen in these STIS spectra. We also investigate the relationship between the  $b$ -parameter distribution and the temperature of the IGM.

##### 4.1. The Temperature-Density Relation

At high redshift, there is a tight relationship between density and temperature  $T$  in the gas

producing the Ly forest, arising from the balance between photoionization heating and adiabatic cooling due to Hubble expansion (e.g. Hui & Gnedin 1997). At low redshift, shocks have heated a significant fraction of even diffuse intergalactic baryons above the equilibrium photoionization temperatures, diluting this tight relation (e.g. Cen & Ostriker 1999, DHKW). However, this shock-heated gas tends to have a low ionization fraction, and hence is less likely to give rise to Ly absorbers, while a substantial amount of baryonic matter remains in the cool, diffuse IGM (see Figure 1 in D01). Thus Ly absorbing gas may still have a reasonably tight  $T$  relation.

Figure 4 shows the temperature  $T$  vs. density  $\rho$  of all absorbers identified in our 40 artificial spectra. The density and temperature of an absorber are taken to be those at the location of the absorber's maximum optical depth, and the density is shown in units of the mean baryonic density at the absorber redshift. A significant fraction of the absorbers lie along a relatively tight relation in

$T$  space arising from photoionization, but there are also many shock-heated absorbers at higher  $T$ . The photoionized absorbers follow the fitting formula

$$T = 5000 \rho^{0.6} \text{ K}; \quad (3)$$

shown as the dashed line, whose slope is similar to that seen at high redshift (Croft et al. 1998). For comparison, we show contours encompassing 50% and 90% of all gas in our simulation. In the density range of STIS Ly absorbers, the absorbers' range of temperatures is significantly smaller than that of all baryons. Evidently, Ly absorbers preferentially (though not uniquely) trace out gas in an equilibrium photoionized state.

##### 4.2. Column Density vs. Gas Density

The FGPA indicates a power-law relationship between the optical depth and the underlying gas density. At low redshift, this relationship becomes contaminated by hot gas that lies on the  $T$  relation as seen in Figure 4, resulting in absorbers with more widely varying ionization fractions, and hence more widely varying underlying densities.

Figure 5 shows plots of column density  $N_{\text{HI}}$  vs. density of underlying gas for the absorbers identified in the 40 artificial spectra. As suggested

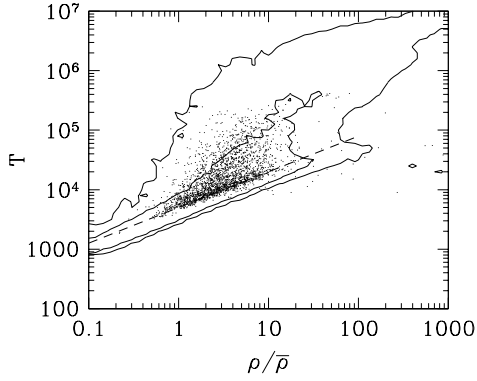


Fig. 4. | Temperature vs. density for absorbers from our artificial spectra. The contours enclose 50% and 90% of all gas particles in our simulation. These contours indicate that while an important shock-heated population is present, the Ly absorbers preferentially sample gas in the photoionized regime. The dashed line shows a fit to the photoionized absorbers, given in equation (3).

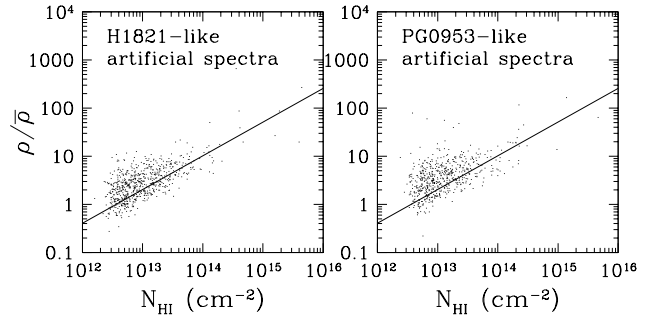


Fig. 5. | Column density  $N_{\text{HI}}$  vs. density in units of the mean  $\rho/\bar{\rho}$ , for absorbers in our artificial spectra. Left and right panels show results from H1821-like and PG0953-like artificial spectra, respectively. The line shows the relation given in equation (4).

by Figure 10 of DHKW, there is substantially greater scatter at low redshift as compared to high redshift. The line shows a similar fit to that in DHKW,

$$b = 12 \frac{N_{\text{HI}}}{10^{14} \text{cm}^{-2}}^{0.7} 10^{0.4z}; \quad (4)$$

corrected for the difference in  $N_{\text{HI}}$  used (discussed further in §5). This is a reasonable fit to the artificial STIS absorbers, though there is a hint of greater scatter than in the  $z = 0$  absorber population of DHKW. This may be because DHKW used  $S/N = 30$  per pixel, whereas our STIS spectra have  $S/N \approx 15$  per pixel, resulting in larger errors in attempting to obtain  $N_{\text{HI}}$ , especially at lower column densities. In Figure 5, the left and right panels show the results from H1821-like and PG 0953-like artificial spectra, respectively. The most deviant outliers in density (at low column densities) arise in the lower- $S/N$  PG 0953-like spectra, indicating that  $S/N$  issues may be important.

Given the large scatter, it is difficult to unambiguously assign an underlying density to an absorber of a given  $N_{\text{HI}}$ , though a trend clearly exists. While higher quality data may tighten this relation somewhat, as of now it appears the FGPA is not nearly as tight a relation at low redshift as compared to high- $z$ . Thus techniques such as recovery of the mass power spectrum (Croft et al. 1998) will face greater challenges in this regime.

#### 4.3. The Temperature of the IGM

Since higher column density systems arise from higher density gas, and higher density gas has higher temperatures, one would expect that  $b$  should be correlated with  $N_{\text{HI}}$ . In particular, the smallest  $b$  parameters at a given  $N_{\text{HI}}$  should mainly reflect the temperature of the underlying absorbers, as thermal broadening should dominate in the narrowest lines. This fact has been used at high redshift to constrain the temperature and "equation of state" (i.e. the  $T$  relation, Hui & Gnedin 1997) of the IGM (Schaye et al. 1999; McDonald et al. 2000a), and a similar argument has been extended to low redshift as well (Ricotti, Gnedin & Shull 2000). It is conceivable that recovering the IGM temperature is actually easier at low- $z$ , because at high redshift, narrow lines can arise from Voigt profiling the asymmetric wings of larger lines, and may be confused for

true narrow absorbers. This occurs much less frequently in the sparser low redshift forest.

Figure 6 shows a plot of  $N_{\text{HI}}$  vs.  $b$  for the absorbers identified in PG 0953+415 and H1821+643 (left panel) and absorbers in our artificial spectra (right panel). The dashed curve shows a running median of  $b$  parameters with  $N_{\text{HI}}$ , with variance in each bin. There is a clear trend for larger  $b$  parameters at larger column densities, as would be expected by the above argument.

We can quantify this relation as follows. In §4.2 we confirmed that equation (4) is a reasonable fit to STIS absorbers (though with large scatter). Equation (3) gives our fit to photoionized absorbers, which are the coolest at any given density. Combining these relations and using  $b = \sqrt{2k_B T/m_p}$  for pure thermal broadening, we obtain an estimate for the minimum  $b$  parameter as a function of column density and redshift:

$$b_{\text{thermal}} = 19 \frac{N_{\text{HI}}}{10^{14} \text{cm}^{-2}}^{0.21} 10^{0.12z} \text{ km/s}; \quad (5)$$

This relation is shown as the solid line in the two panels of Figure 6, for  $z = 0.17$  (the mean redshift of the observed sample). It is a good approximation to the lower envelope of absorber  $b$  parameters for  $N_{\text{HI}} > 10^{13.3} \text{cm}^{-2}$  in our artificial spectra (right panel). Below this column density, presumably blending is more frequent, and narrow lines from line wings dilute this relationship. Also, noise can cause some weak lines to appear narrower than they really are, since weaker lines have larger profiling uncertainties. As seen in the left panel, equation (5) is consistent with a lower envelope for all but the weakest STIS absorbers as well, though a larger sample of absorbers will be required before such a relation may be recovered directly from the observations.

Comparing the solid line (pure thermal broadening) with the dashed line (median  $b$ ) in Figure 6 suggests that thermal broadening is responsible for a substantial portion of the absorber widths, with  $b_{\text{thermal}} \approx 0.7b$  for a typical absorber. This fraction remains fairly constant with  $N_{\text{HI}}$ . This is also seen in Figure 3, where the dotted line shows the histogram of thermal widths for  $N_{\text{HI}} > 10^{13} \text{cm}^{-2}$  absorbers; its median value is  $\approx 15$  km/s. The contribution from thermal broadening is therefore greater than at high redshift, where bulk flow

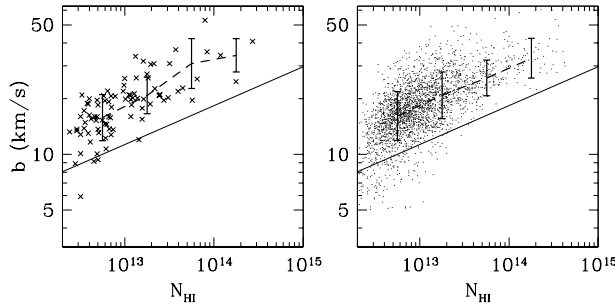


Fig. 6. |  $N_{\text{HI}}$  vs.  $b$ -parameter for STIS-observed absorbers (left panel) and absorbers in 40 artificial spectra (right panel). The thick dashed line shows the median  $b$  in four bins of  $N_{\text{HI}}$ , with variance computed within each bin. The solid line shows thermal broadening as a function of  $N_{\text{HI}}$ , given by equation (5).

broadening dominates (e.g. Hemquist et al. 1996; Schaye et al. 1999).

Equation (5) was obtained from fits to the particular simulation used here; it is not true in general. In order to measure the temperature of the IGM unambiguously, it is important to test equations (3) and (4) over a wider range of parameter space. Nevertheless, the good agreement with the  $b$ -parameter distribution, as well as the significant contribution of thermal broadening to this distribution, suggests that these simulations are accurately characterizing the "equation of state" of the low- $z$  IGM. Our measurement is given by equation (3), indicating a temperature of  $\sim 5000$  K at the mean density. Increasing the temperature by more than a factor of two would produce thermal  $b$ -parameters alone that are larger than observed, so we place an upper limit at  $T(\rho) \sim 10^4$  K. Since this fit is only for our current simulation, it is subject to the uncertainties in modeling, but at least at high redshift measurements of  $T$  are not very sensitive to such uncertainties (Theuns, Schaye, & Haehnelt 2000). Note that we are measuring here the temperature of equilibrium photoionized Ly forest absorbers only, and this does not exclude the possibility that the IGM contains a component of hotter gas that may give rise to, say, O VI absorption (Tripp, Savage, & Jenkins 2000).

A similar technique has already been used to determine the temperature of the IGM from GHRIS data, obtaining a value of  $T(\rho) = 4700$  K for  $J_0 = 10^{23} \text{ erg s}^{-1} \text{ cm}^{-2} \text{ sr}^{-1} \text{ Hz}^{-1}$  (Ricotti, Gnedin & Shull 2000), in agreement with our result. With more STIS data and better simulations, this type of analysis should be able to robustly measure the temperature of the low-redshift IGM in the near future.

## 5. Preliminary Constraints on $N_{\text{HI}}$

As stated in §3, the agreement between the observed and simulated column density distribution amplitude is in principle a test of the ionization state of the absorbing gas. Because the absorbing gas for  $N_{\text{HI}} \sim 10^{14} \text{ cm}^{-2}$  is optically thin,  $\tau_{\text{Ly}} \propto N_{\text{HI}} / n_{\text{HI}} \propto n_{\text{HI}}^{-1}$ , so changing the ionization fraction of Ly forest absorbers will shift the simulated  $f(N_{\text{HI}})$  in the horizontal direction, and alter the agreement with observations.

It is straightforward to determine the shift in

$N_{\text{HI}}$  that produces the best agreement with observations, then translate that into a value for  $\Gamma_{\text{HI}}$ . This yields  $\Gamma_{\text{HI}} = 10^{13.3 \pm 0.12} \text{ s}^{-1}$  at an average redshift of  $z = 0.17$ , up by  $0.2$  dex from the value of  $\Gamma_{\text{HI}}$  originally used to construct the artificial spectra. Figure 7 shows this value of  $\Gamma_{\text{HI}}$  (filled circle) in relation to other predicted and observed values. The error bars on this value are discussed below. The value derived here is close to the "matched LCDM" curve from DHKW (solid line), since it was this  $\Gamma$  that produced the good agreement with the observed  $f(N_{\text{HI}})$  seen in Figure 2. This value is even closer to that predicted from the evolution of the quasar population by Haardt & Madau (1996, dashed line) and three-fourths of a similar prediction by Fardal, Giroux, & Shull (1998, dotted line) at  $z = 0.17$ . A recent calculation accounting for emission from QSOs, Seyferts and starbursts (Shull et al. 1999) is shown as the diamond at  $z = 0$ , and is quite consistent with our measurement.

Figure 7 also shows various measurements that constrain  $\Gamma_{\text{HI}}$  at low redshift (a more complete discussion may be found in Shull et al. 1999). The open circle at  $z = 0.5$  comes from the proximity effect (Kulkarni & Fall 1993), the open square comes from modeling the radial truncation of HI in the isolated spiral NGC 3198 (Maloney 1993; Dove & Shull 1994), and the two downward triangles show upper limits from HI emission due to photoevaporation of nearby HI clouds (Vogel et al. 1995; Donahue, Aldering & Stocke 1995). An actual measurement using this last technique is in preparation (R. Weymann, private communication). Tumlinson et al. (1999) used metal absorption line ratios in the halo gas of NGC 3067 to model the required photoionizing background, and their lower limit is shown as the upward triangle. Note that all these methods assume that the ionizing radiation is metagalactic and not local, despite measuring the field close to an observable object. Conversely, weak Ly absorbers are typically far from galaxies (Stocke et al. 1995; Tripp, Lu, & Savage 1998). Additionally, our statistical errors are smaller than those of any of the above measurements, but as we now discuss, our modeling uncertainties dominate.

The FGPA (eq. 1) indicates that  $\Gamma$  depends on the density of the absorbing gas in addition to  $\Gamma_{\text{HI}}$ . The exponent of this dependence is approximately

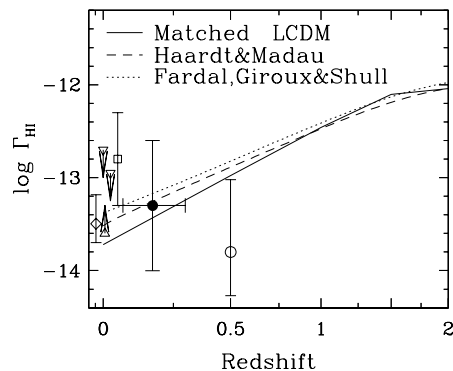


Fig. 7. | Our measurement of  $\Gamma_{\text{HI}}$  (filled circle) from the column density distribution of the Ly forest. The errors are dominated by modeling uncertainties; the horizontal errors show the redshift range of absorbers in our STIS spectra. Predictions for the evolution of  $\Gamma_{\text{HI}}$  are shown as dashed (Haardt & Madau 1996) and dotted (Fardal, Giroux, & Shull 1998) lines. Solid line shows the "matched LCDM" rate that reproduces the evolution of  $dN/dz$  for  $W_r > 0.24A$  FOS absorbers (DHKW). This  $\Gamma_{\text{HI}}$  was the one used to generate our artificial STIS spectra. Various measurements are indicated: proximity effect (open circle, Kulkarni & Fall 1993); HI truncation in spiral galaxy (open square, Maloney 1993; Dove & Shull 1994); photoevaporation of HI cloud (downward triangles, upper limits, Vogel et al. 1995; Donahue, Aldering & Stocke 1995); modeling of metal line ratios (upward triangle, lower limit, Tumlinson et al. 1999). Some points near  $z = 0$  have been offset slightly for clarity.

1.6 at high redshift. In the previous section we showed that low redshift absorbers are consistent with this relation, though the spread is significantly greater. What is less certain is how the density of the absorbing gas varies as one changes  $\Omega_b$ , cosmology, and numerical parameters in the simulations.

At high redshift, nearly all the baryons are in the Ly forest, so the FGPA can be used to directly probe  $\Omega_b$  (Rauch et al. 1997; Weinberg et al. 1997). At low redshift, the fraction of gas giving rise to Ly absorbers is significantly smaller ( $\sim 20\%$ ; Penton, Shull, & Stocke 2000), because many of the baryons have moved into other phases (D HKW, Cen & Ostriker 1999, D01). Though modeling uncertainties are large (as we discuss below), the cosmological simulations generally predict that at the present epoch roughly 1/3 of the baryons are in diffuse photoionized gas, 1/3 are in the shock-heated IGM, and 1/3 are in virialized systems such as galaxies and clusters (see D01 and references therein). Studies of low- $z$  Ly absorbers suggest that the diffuse photoionized IGM contains a considerable fraction of the baryons (Shull, Stocke & Penton 1996; Penton, Shull, & Stocke 2000). The shock-heated IGM is more challenging to detect, but detections of O VI at low redshift suggest that the predicted hot gas is indeed present (e.g. Tripp, Savage, & Jenkins 2000), though since O VI absorption can occur in photoionized gas and Ly lines can originate in hot gas (see, e.g., x4 in Tripp & Savage 2000), there may be some double-counting in estimates of baryon reservoirs traced by various QSO absorbers.

Exactly how much baryonic matter remains in gas traced by Ly absorbers is uncertain. One estimate may be obtained if we consider that low- $z$  absorbers preferentially arise in the so-called "diffuse" (i.e. photoionized) phase of D HKW and D01, as suggested by Figure 4. In D01, the baryon fraction in this phase varies by as much as a factor of two ( $\sim 20\text{--}40\%$ ) among their simulations having various volumes, resolutions, and hydrodynamic algorithms. Furthermore, those simulations all were based on  $\Lambda$ CDM universes with similar  $\Omega_b$ . While this world model has gained much support recently (Bahcall et al. 1999), D HKW's analysis of several different cosmologies also indicates a possible variation of a factor of  $\sim 1.5$  in the

baryon fraction in this phase due to the differing rates of structure formation. Additionally, there is some uncertainty in  $\Omega_b$  itself, and uncertainties in  $H_0$  come into play as well since the observed quantity is usually the combination  $\Omega_b h^2$ . Due to these variations, combined with  $\Omega_b^{-1.6} = \dot{J}_{\text{HI}}$ , our best estimate for a 1- $\sigma$  systematic uncertainty in the determination of  $\dot{J}_{\text{HI}}$  is roughly a factor of

5. Clearly this dominates over the statistical error quoted above.

Thus we will claim a preliminary measurement of  $\dot{J}_{\text{HI}} = 10^{13.3 \pm 0.7} \text{ s}^{-1}$  from the Ly forest, at  $z = 0.17$ . This value is shown as the filled circle in Figure 7; the horizontal error bar indicates the redshift range covered by our STIS spectra. For the spectral shape proposed by Fardal et al. (similar to that of Haardt & Madau and approximately  $\nu^{-1.8}$ ), this translates to  $J = 1.9 \times 10^{23} \text{ erg s}^{-1} \text{ cm}^{-2} \text{ sr}^{-1} \text{ Hz}^{-1}$  at 912 Å. Our preliminary result would clearly benefit from improved simulations to better quantify the uncertainties involved. Unfortunately, analytic or semi-analytic methods such as that of Hui, Gnedin, & Zhang (1997) are not applicable to this problem, since the physics of the diffuse IGM at low- $z$  involves a complex dynamical interplay of non-equilibrium structures. A proper quantification would involve performing a suite of large-scale hydrodynamic simulations exploring the relevant parameters, something that is beyond our current computational capability. Still, despite the large and poorly quantified uncertainties in the value derived here, ours is among the best observational constraints on the metagalactic HI photoionization rate to date, and others hope that a more precise determination may be forthcoming soon.

## 6. Conclusions

We have examined the intergalactic Ly absorber population in STIS spectra of PG 0953+415 and H 1821+643, and compared it to that in artificial spectra drawn from a cosmological hydrodynamic simulation of a  $\Lambda$ CDM universe. The good spectral resolution (7 km/s) and relatively high S/N of these STIS spectra yield an unprecedented view into the weak absorber population at low redshift. We find:

The column density distributions agree quite well in slope and amplitude. The measured

slope is  $\approx 2.04 \pm 0.23$ , considerably steeper than that seen at high redshift ( $\approx 1.5$ ), indicating that strong absorption line systems have evolved away faster than weak ones.

The b-parameter (line width) distributions agree quite well, with an intrinsic median b-parameter of  $\approx 21$  km/s. This value is lower than that seen at high redshift, suggesting that the IGM has cooled and/or bulk flow broadening has lessened. The median b-parameter increases with  $N_{\text{HI}}$ , indicating that denser IGM gas is hotter. From a comparison of b-parameters with the expected thermal line width, thermal broadening has an increased contribution to line widths at low  $z$ , with  $b_{\text{thermal}} \approx 0.7b$ .

Ly absorbers preferentially arise in gas having temperatures close to that expected from photoionization, with  $T \approx 10^6$ , though there is substantial scatter to higher temperatures due to absorbers arising in the shock-heated IGM.

The density-column density relation, a.k.a. the fluctuating Gunn-Peterson approximation, is considerably less tight at low redshift than at high  $z$ . A trend still exists, consistent with that seen at high redshift, but shows greater scatter.

The minimum b-parameter as a function of column density faithfully yields the temperature-density relation in the IGM. The simulation analyzed here suggests  $T \approx 5000$  K, with an upper limit of  $10^4$  K, for Ly absorbing gas at the cosmic mean density.

The amplitude of the column density distribution may be used to place constraints on  $N_{\text{HI}}$ , the metagalactic H I photoionization rate at low  $z$ . We find, at  $z \approx 0.17$ ,  $\Gamma_{\text{HI}} \approx 10^{13.3 \pm 0.7} \text{ s}^{-1}$ , with systematic uncertainties in modeling being the dominant source of error.

In summary, weak Ly absorbers in the low-redshift IGM seen with STIS appear to be physically similar to high redshift Ly absorbers, arising in non-equilibrium large-scale structures that

are highly photoionized by the metagalactic UV flux, as suggested by DHKW. Uncertainties from our current simulation limit our ability to extract all possible quantitative information contained even in this small sample of STIS spectra, so improved simulations will be required to confirm the results presented here. Still, these preliminary results indicate that we are close to understanding the low redshift Ly forest at a level similar to what has been achieved at high redshift. This would be a remarkable achievement for studies of the nearby intergalactic medium using ultraviolet spectroscopy, and analogous to what has transpired recently with high- $z$  forest studies, promises to open up a new realm for observational tests of theories of cosmology, structure formation, and the evolution of intergalactic baryons.

We thank David Weinberg and Ray Weymann for helpful discussions. This research made use of data reduction programs developed by the STIS IDT, and we thank the STIS Team for allowing us to use this software.

This work was supported in part by NASA ATP grant NAG 5-7066. Support for this work was also provided by NASA through grant number GO-08165.01-97A and Hubble Fellowship grant number GO-07465.01-A from the Space Telescope Science Institute, which is operated by AURA, Inc., under NASA contract NAS5-26555.

## REFERENCES

- Bahcall, J. N., Jannuzi, B. T., Schneider, D. P., Hartig, G. F., Bohlin, R., & Junkkarinen, V. 1991, *ApJ*, 377, L5
- Bahcall, J. N., et al. 1993, *ApJS*, 87, 1
- Bahcall, J. N., et al. 1996, *ApJ*, 457, 19
- Bahcall, N., Ostriker, J. P., Perlmutter, S., & Steinhardt, P. J. 1999, *Science*, 284, 1481
- Burles, S. & Tytler, D. 1998, *ApJ*, 507, 732
- Bryan, G. L., Machacek M., Anninos P., & Norman M. L., 1999, *ApJ*, 517, 13
- Cen, R. & Ostriker, J. P. 1999, *ApJ*, 514, 1
- Chen, H.-W., Lanzetta, K. M., Webb, J. K., & Barcons, X. 1998, *ApJ*, 498, 77

- Croff, R. A. C., Weinberg, D. H., Katz, N., & Hemquist, L. 1998, ApJ, 495, 44
- Croff, R. A. C., DiMatteo, T., Dave, R., Hemquist, L., Katz, N., Fardal, M. A., & Weinberg, D. H. 2000, ApJ, submitted, astro-ph/0010345
- Dave, R., Cen, R., Ostriker, J. P., Bryan, G. L., Hemquist, L., Katz, N., Weinberg, D. H., Norman, M. L., & O'Shea, B. 2001, ApJ, in press, astro-ph/0007217 [D01]
- Dave, R., Hemquist, L., Katz, N., & Weinberg, D. H. 1999, ApJ, 511, 521 [DHW]
- Dave, R., Hellsten, U., Hemquist, L., Katz, N., & Weinberg, D. H. 1999, ApJ, 509, 661
- Dave, R., Hemquist, L., Weinberg, D. H., & Katz, N. 1997, ApJ, 477, 21
- Dave, R., Dubinski, J., & Hemquist, L. 1997, NewAstr, 2, 277
- Donahue, M., Aklaring, G., & Stocke, J. T. 1995, ApJ, 450, L45
- Dove, J. B., & Shull, J. M. 1994, ApJ, 423, 196
- Fardal, M., Giroux, M. L., & Shull, J. M. 1998, AJ, 115, 2206
- Giroux, M. L., & Shull, J. M. 1997, AJ, 113, 1505
- Haardt, F., & Madau, P. 1996, ApJ, 461, 20
- Haehnelt, M. G., & Steinmetz, M. 1998, MNRAS, 298, L21
- Heap, S. R., Williger, G. M., Smette, A., Hubeny, I., Sahu, M. S., Jenkins, E. B., Tripp, T. M., & Winkler, J. N. 2000, ApJ, 534, 69
- Hemquist, L., Katz, N., Weinberg, D. H., & Miralda-Escudé, J. 1996, ApJ, 457, L51
- Hu, E. M., Kin, T. S., Cowie, L. L., Songaila, A., & Rauch, M. 1995, AJ, 110, 1526
- Hui, L., & Gnedin, N. Y. 1997, MNRAS, 292, 27
- Hui, L., Gnedin, N., & Zhang, Y. 1997, ApJ, 486, 599
- Jannuzzi, B. T., et al. 1998, ApJS, 118, 1
- Kin, T. S., Hu, E. M., Cowie, L. L., & Songaila, A. 1997, AJ, 114, 1
- Kin, T. S., Cristiani, S., & O'dorico, S. 2000, A & A, submitted
- Kinble, R. A., et al. 1998, ApJ, 492, L83
- Kirkman, D., & Tytler, D. 1997, ApJ, 489, L123
- Kulkarni, V. P., & Fall, S. M. 1993, ApJ, 413, 63
- Lanzetta, K. M., Tumshak, D. A., & Wolfe, A. M. 1987, ApJ, 322, 739
- Lu, L., Sargent, W. L. W., Ombse, D. S., & Takada-Hidai, M. 1996, ApJ, 472, 509
- Lynds, R. 1971, ApJ, 164, L73
- Machacek, M. E., Bryan, G. L., Meiksin, A., Anninos, P., Thayer, D., Norman, M., & Zhang, Y. 2000, ApJ, 532, 118
- Maloney, P. 1993, ApJ, 414, 41
- McDonald, P., Miralda-Escudé, J., Rauch, M., Sargent, W. L. W., Barlow, T. A., Cen, R., & Ostriker, J. P. 2000a, ApJ, 543, 1
- McDonald, P., Miralda-Escudé, J., Rauch, M., Sargent, W. L. W., Barlow, T. A., & Cen, R. 2000b, ApJ, submitted, astro-ph/0005553
- Miralda-Escudé, J., Cen, R., Ostriker, J. P., & Rauch, M. 1996, ApJ, 471, 582
- Morris, S. L., Weymann, R. J., Savage, B. D., & Gilliland, R. L. 1991, ApJ, 377, L21
- Ostrum, P. J., Carswell, R. F., & Theuns, T. 2000, 529, L73
- Penton, S. V., Shull, J. M., & Stocke, J. T. 2000, ApJ, 544, 150
- Rauch, M., Haehnelt, M. G., & Steinmetz, M. 1997, ApJ, 481, 601
- Rauch, M., Miralda-Escudé, J., Sargent, W. L. W., Barlow, T. A., Hemquist, L., Weinberg, D. H., Katz, N., Cen, R., Ostriker, J. P. 1997b, ApJ, 489, 7
- Rauch, M. 1998, ARA & A, 36, 267
- Ricotti, M., Gnedin, N. Y., & Shull, J. M. 2000, ApJ, 534, 41
- Schaye, J., Theuns, T., Rauch, M., Efsthathiou, G., & Sargent, W. L. W. 1999, MNRAS, 310, 57

- Shull, J. M., Stocke, J. T., & Penton, S. 1996, *AJ*, 111, 72
- Shull, J. M., Roberts, D., Giroux, M. L., Penton, S. V., & Fardal, M. A. 1999, *AJ*, 118, 1450
- Shull, J. M., Giroux, M. L., Penton, S. V., Tumlinson, J., Stocke, J. T., Jenkins, E. B., Moos, H. W., Oegerle, W. R., Savage, B. D., Sembach, K. R., York, D. G., Green, J. C., & Woodgate, B. E. 2000, *ApJ*, 538, L13
- Songaila, A. & Cowie, L. L. 1996, *AJ*, 112, 335
- Stocke, J. T., Shull, J. M., Penton, S., Donahue, M., & Carilli, C. 1995, *ApJ*, 451, 24
- Theuns, T., Leonard, A., & Efsthathiou, G. 1998, *MNRAS*, 297, L49
- Theuns, T., Leonard, A., Efsthathiou, G., Pearce, F. R., & Thomas, P. A. 1998, *MNRAS*, 301, 478
- Theuns, T., Schaye, J., & Haehnelt, M. G. 2000, *MNRAS*, 315, 600
- Tripp, T. M., Lu, L., & Savage, B. D. 1998, *ApJ*, 508, 200
- Tripp, T. M. & Savage, B. D. 2000, *ApJ*, 542, 42
- Tripp, T. M., Savage, B. D., & Jenkins, E. B. 2000, *ApJ*, 534, L1
- Tripp, T. M., et al. 2001, in preparation
- Tumlinson, J., Giroux, M. J., Shull, J. M., & Stocke, J. T. 1999, *AJ*, 118, 2148
- Vogel, S., Weymann, R., Rauch, M., & Hamilton, T. 1995, *ApJ*, 441, 162
- Vogt, S. S., et al. 1994, *SPIE*, 2198, 326
- Weinberg, D. H., Hemquist, L., Miralda-Escudé, J., & Katz, N., 1997, *ApJ*, 490, 564
- Weymann, R., et al. 1998, *ApJ*, 506, 1
- Wu, K. K. S., Fabian, A. C., & Nulsen, P. J. E. 2000, *MNRAS*, submitted, astro-ph/9910122
- Zhang, Y., Anninos, P., & Norman, M. L. 1995, *ApJ*, 453, L57